2006 IEEE International Conference on
Multisensor Fusion and Integration for Intelligent Systems
September 3-6, 2006, Heidelberg, Germany

Detection of Circular Defects on Varnished or Painted Surfaces by Image Fusion

Ana Pérez Grassi, Miguel Ángel Abián Pérez, Fernando Puente León, and Rosa María Pérez Campos

Abstract— **Varnishing and painting are quite delicate processes susceptible to failures. This becomes especially critical whenever an aesthetic finish is decisive for the final product. Such is the case, for example, in production of furniture, musical instruments, and paper, among many others. Dozens of different defects with very varied shapes can affect varnished or painted surfaces. However, an important group of them presents a mere circular geometry. Circular defects can have very different sizes and are only partially visible under certain illumination conditions. These characteristics complicate the quality control of varnished or painted surfaces, for which an automated solution does not exist. On the contrary, this work is performed by human operators, which yields to a long, expensive and subjective inspection process. In order to implement an automated surface inspection, different lighting directions and a priori knowledge on the defect symmetry are combined. The image series, resulting of sampling the illumination space, presents the complete information of defects, but distributed on its pictures. To collect all this information, an iterative algorithm based on a multidimensional correlation filter is proposed, which enables a reliable identification of circular defects with arbitrary diameters. Moreover, the successful detection and identification of these defects is not affected by the surface texture.**

I. Introduction

Many factors can cause defects on varnished or painted surfaces—e.g. inappropriate room conditions, low-quality raw materials, defective machines or the usage of incompatible chemical products. A huge amount of economic loss is incurred every year as a result of failures on painted or varnished surfaces not detected in time. Such surfaces are only partly controlled by human operators through a long procedure of visual inspection, not assuring a zero defects product, slowing down the production cycle, and increasing both production and quality control costs. Additional cost may also be expected if the varnishing or painting process must be interrupted to perform the necessary repairs. In conclusion, the cost to fix finish failures far outweighs the initial cost of varnishing or painting. Three of the most important defects, because of their frequent appearance and economic impact, are craters, bubbles, and blisters; see Fig. 1 [1]. These defects have different causes, but they feature a common characteristic: circular geometry.

A blister appears as a dome-like raised area containing water or other liquids. Blistering is due to the local loss of adhesion and lifting of the film from the underlying substrate, usually because painting was performed before the previous coat has dried thoroughly or due to excessive heat or grease under the paint. A bubble is also a dome-like raised area, but contains air or solvent vapor. Bubbling is often caused by applying the finish too thick, too heavily, or by an excessive brushing without topping off. Craters are small, shallow, bowl-shaped depressions in the coating film; these depressions were once covered by bubbles. Viewed under magnification, these depressions frequently have drops, particles, or other material at their centres and raised circular edges. Usually, they are produced because there is an incompatibility between the coating and the substrate or the base coat, which causes the coating rejection [2], [3].

Circular defects present different diameters (approx. 0.2–4 mm). Moreover, the size of the smaller ones may present the same order of magnitude as other finishing irregularities, which might or not be considered defects, and normal wood texture details (in the case of transparent varnish). These defects are only visible under appropriate lighting directions. This can be appreciated in Fig. 2, which shows the same damaged surface under different illumination conditions. In this case, the image corresponds to a wood surface treated with a transparent varnish which contains two craters. The right-most picture was taken under diffuse light, while the left-most one under directional light.

The small crater on the inferior part of the picture (see the pointing arrow) is practically imperceptible under diffuse illumination: diffuse light can be described as a superposition of directional light sources, which may result in a destructive overlapping of light and shadow. In the case under consideration, this causes a decrease of the image contrast [4].

On the other hand, the local image contrast is higher under directional light. However, the defects are only partially visible. The craters on the right-most picture can be distinguished only through highlights on their rims. The position of these highlights evidently depends on the used lighting direction.

Additionally, Fig. 2 shows that if the used finishing film is transparent, the texture of the underlying surface is visible and constitutes a noisy background which may mask out some defects. This makes conventional methods inappropriate for a reliable detection of defects.

II. Image Acquisition

To achieve maximal contrast, pictures of the varnished surfaces are taken under directional illumination, which is realized with a distant light source. The experimental setup

Ana Pérez Grassi and Fernando Puente León are with the Technische Universität München, Fachgebiet Verteilte Messsysteme, D-80333 Munich, Germany {a.perez, f.puente}@tum.de

Miguel Ángel Abián Pérez and Rosa María Pérez Campos are with AIDIMA – Furniture, Wood and Packaging Technology Institute, E-46980 Paterna (Valencia), Spain {mabian, rperez}@aidima.es

1-4244-0567-X/06/$20.00 ©2006 IEEE.

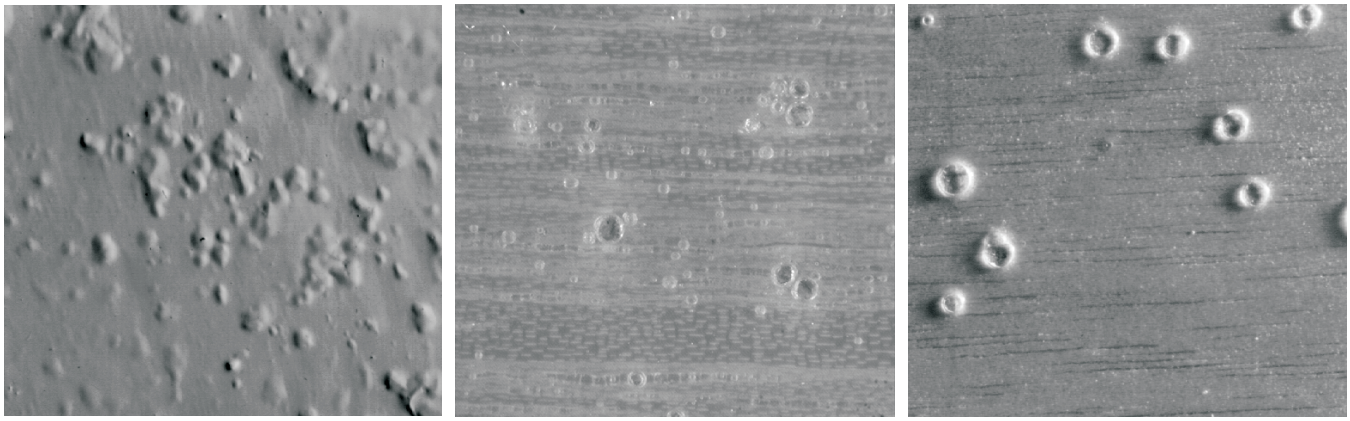

Fig. 1. Different varnished surfaces featuring circular defects: blisters (left), bubbles (middle), and craters (right).

used for the image acquisition allows the variation of the light source position, while the camera is fixed with its optical axis parallel to the z-axis of the Cartesian coordinate system; see Fig. 3. The main idea is to take a series of images sampling the illumination space, which is defined as the space of all possible illumination directions $\mathbf{b}$, given by the azimuth φ and the elevation angle θ.

Circular defects typically feature a border, and either a central cavity (craters) or a dome (blisters and bubbles). In contrast, intact varnish can be assumed to form a perfectly planar surface. Figure 4 shows characteristic profiles of both intact and damaged surfaces.

Varnished surfaces behave partly like a mirror, if they are illuminated directionally. In this case, the incident light beam is predominately reflected in a direction depending on the local normal vector $\mathbf{n}$ of the surface. If $\mathbf{n}$ and $\mathbf{b}$ are not parallel, a non-defective surface appears dark to the camera, whose optical axis coincides with the normal vector, if $\theta > 0$ holds. On the other hand, in the presence of defects, due to the local variation of the normal vector $\mathbf{n}$, the reflected

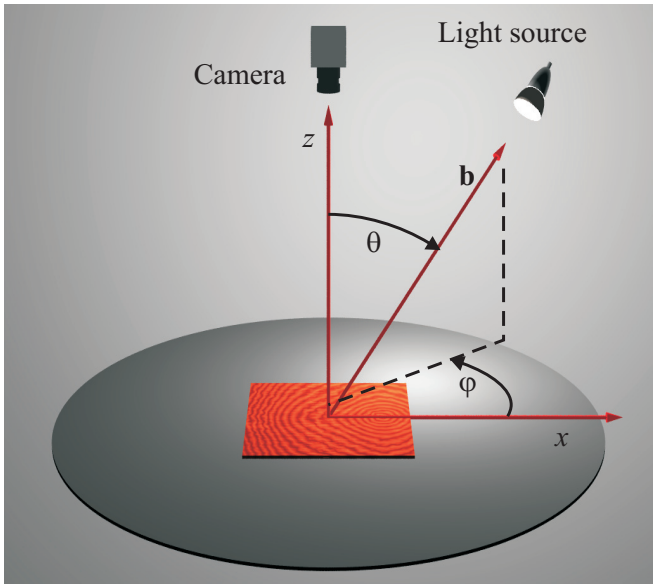

Fig. 3. Image acquisition setup.

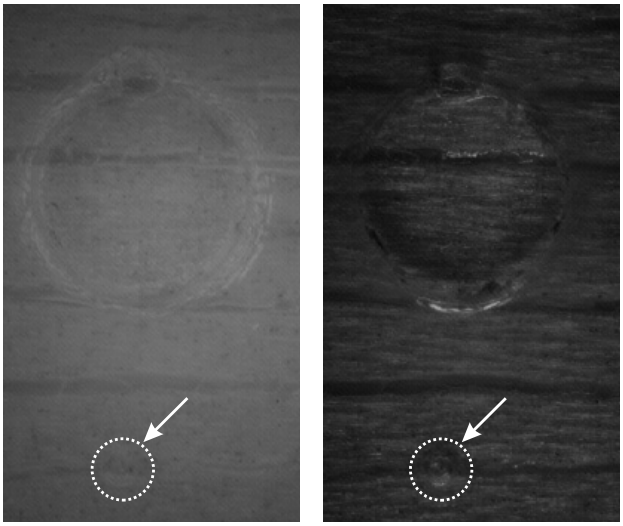

Fig. 2. Craters under diffuse (left) and directional (right) light.

light beam might partly be spread to the camera. This effect becomes visible in the form of highlights in Fig. 2 (right).

Because of the local variation of the surface topography (more exactly, of the normal vector $\mathbf{n}$ along the perimeter of the defects), highlights do not appear along the complete perimeter, but only within a sector of it. If the defect is illuminated using a constant elevation angle θ whereas the azimuth φ is gradually varied, this brighter sector rotates around the defect. Since each image obtained with a determined illumination azimuth φ presents a fraction of the defect border, the information contained in a single image is not sufficient to enable a reliable detection. Consequently, to obtain the information about the whole perimeter, a series $\mathcal{S}$ of B images using a systematic variation of the azimuth angle φ must be recorded:

$$\mathcal{S} = \{s(\mathbf{x}, \varphi_i),\ i = 0, \ldots, B-1\}\,, \tag{1}$$

$$\varphi_i = \varphi_0 + i\Delta\varphi\,, \qquad 0 \le \varphi_i < 2\pi\,, \tag{2}$$

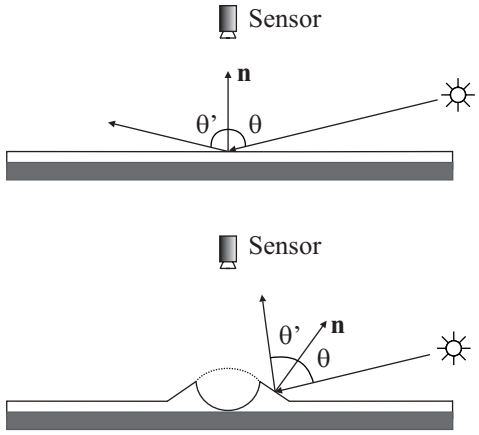

Fig. 4. Reflection characteristics of an intact and a defective surface.

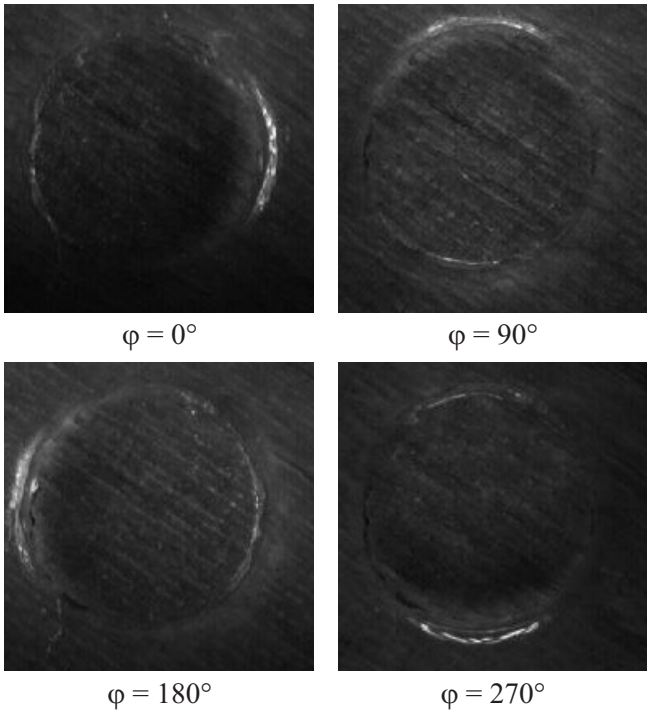

Fig. 5. Image series of a varnished wood surface showing a crater, illuminated from a fixed elevation angle θ and a variable azimuth φ.

where $\mathbf{x} = (x, y)^{\mathrm{T}}$. For example, Fig. 5 shows an image series ($B = 4$) of a varnished wood substrate featuring a crater. The pictures were taken with a variable illumination azimuth ($\Delta\varphi = 90°$) and a fixed elevation angle $\theta \approx 80°$.

Finally, the use of an ideal directional light source may demand an extremely dense sampling of the illumination space to avoid loss of relevant information. However, this is not necessary for most practical applications [5]. For our purposes, a spatially extended light source can be successfully applied to detect circular defects.

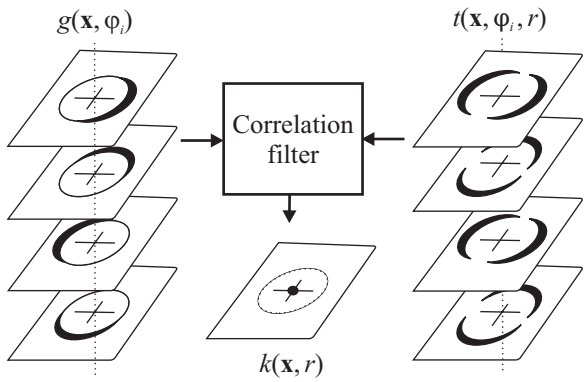

Fig. 6. Correlation of the image series and the corresponding templates for a particular radius.

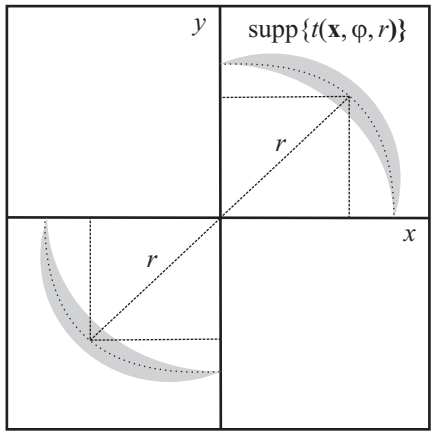

Fig. 7. Support set of the template used for the correlation for $\varphi = 45°$.

III. Detection Strategy

A. Preprocessing

To achieve a robust identification of defects with circular symmetry, it is first necessary to suppress low-frequency grey-value fluctuations caused by illumination inhomogeneities. This suppression is performed using a highpass filter HP{ }, which yields to a locally zero-mean signal [6]:

$$g(\mathbf{x}, \varphi_i) = \mathrm{HP}\{s(\mathbf{x}, \varphi_i)\}\,. \tag{3}$$

After this preprocessing, the defects can be identified by means of the highlights on their perimeters, which present a clearly higher intensity than the background. Although it would be possible, in principle, to detect these highlights with a simple threshold, this strategy does not yield satisfactory results when the substrate texture is visible. Significantly better results are achieved using a correlation filter.

B. Correlation filter in the illumination space

Correlation filters are used in many image processing applications to detect known patterns in the presence of noise [7]. In this case, the known patterns are the highlights along the perimeters of the defects. These highlights move around the defect borders as the illumination direction varies. This effect causes a distribution of the information of interest

along the different images of the series. This characteristic requires to extend the classic correlation filter along one additional dimension—the illumination dimension:

$$k(\mathbf{x}, r) := \sum_{i=1}^{B-1} g(\mathbf{x}, \varphi_i) \circledast t(\mathbf{x}, \varphi_i, r)\,, \tag{4}$$

where $t(\mathbf{x}, \varphi_i, r)$ denotes the template obtained by modeling the features of interest. The correlation filter is not especially sensitive to the exact shape of the template curve [8]. Figure 6 schematises this operation for one defect. The template is a bimodal function with the shape shown in Fig. 7. The two opposite arcs are necessary because, for a given lighting direction, highlights may appear on the external side of the defect border as well as on the opposite internal side. This phenomenon depends on the border curvature. In addition, $t(\mathbf{x}, \varphi_i, r)$ depends not only on the azimuth φ_i, but also on the defect radius r. Therefore, the filter must be reconfigured and executed iteratively for different radii. If an image $g(\mathbf{x}, \varphi_i)$ contains defects with a certain radius r, the correlation result $k(\mathbf{x}, r)$ features a maximum at the centres of the defects; see Fig. 6. To achieve a successful detection of defects with different radii, an adaptive threshold is applied.

In Fig. 6, it becomes evident that $t(\mathbf{x}, \varphi_i, r) = t(\mathbf{x}, \varphi_i + 180°, r)$. For this reason, since all of the operations involved in the calculation of $k(\mathbf{x}, r)$ are linear, image pairs with opposite lighting directions are added first, so that only $B/2$ correlations are necessary to compute $k(\mathbf{x}, r)$.

C. Using circular symmetry to improve detection

Due to the circular symmetry of the defects under consideration, the correlation result for a true positive is predictable. Figure 8(a) shows a 2D correlation between a simulated circular defect with radius r, when illuminated with $\varphi = 45°$, and the corresponding mask $t(\mathbf{x}, \varphi = 45°, r)$. The result presents two areas. The central one is produced by the mask arc and the image arc with the same orientation. The other area, which is separated from the defect centre by approximately $2r$, is originated by the second mask arc, which is rotated by 180° with respect to the first one. Figure 8(b) shows the correlation result for a real surface. In spite of wood texture, simulated and real results look very similar.

When all 2D correlation results are fused according to (4), their central areas are superposed yielding a high peak, and the external areas form a tenuous circle with a radius of approximately $2r$ around the centre; see Fig. 9(a). Only the detection of circular defects presents this characteristic shape. Therefore, this fact can be used to distinguish between false and true positives.

In order to decide whether a point $\mathbf{x}$ is surrounded by a tenuous circle or not, the difference between its intensity $k(\mathbf{x}, r)$ and the average of the neighbourhood set

$$\mathcal{N}(\mathbf{x}) = \{\mathbf{u} \mid r_{\text{int}} \leq \|\mathbf{x} - \mathbf{u}\| \leq r_{\text{ext}}\} \tag{5}$$

around it is computed, where $r_{\text{ext}} = r$, $r_{\text{int}} = \mathrm{b} \cdot r$, and $\mathrm{b} \in [0, 1]$; see Fig. 9(b). Then, a signal $d(\mathbf{x}, r)$ is calculated as follows:

$$d(\mathbf{x}, r) := k(\mathbf{x}, r) - \frac{1}{|\mathcal{N}|} \sum\nolimits_{\mathbf{x} \in \mathcal{N}(\mathbf{x})} k(\mathbf{x}, r)\,, \tag{6}$$

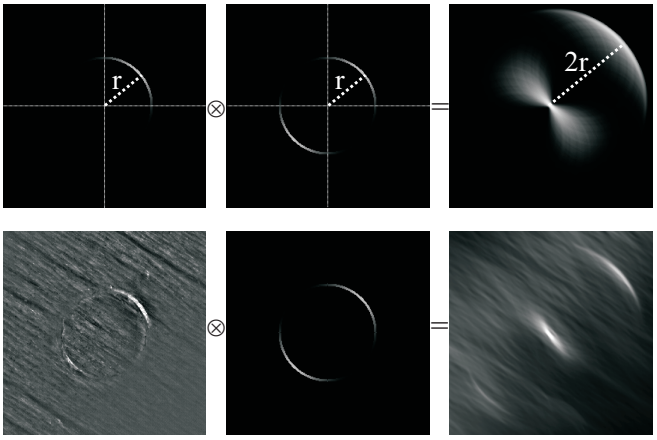

Fig. 8. (a) Correlation result for a simulated case (top). (b) Correlation result for a real crater (bottom).

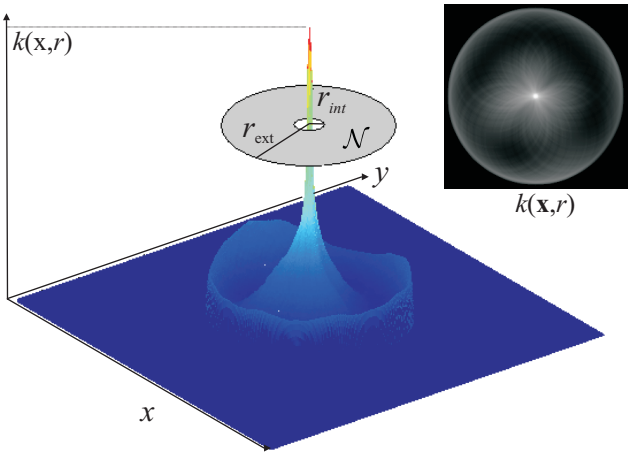

Fig. 9. (a) Superposition of the correlation results for a true positive detection (right). (b) Neighbourhood set $\mathcal{N}$ around a true positive (left).

where $|\mathcal{N}|$ denotes the area of $\mathcal{N}$. To emphasize true positives in $k(\mathbf{x}, r)$, $d(\mathbf{x}, r)$ is fused with $k(\mathbf{x}, r)$ by multiplying both signals:

$$k'(\mathbf{x}, r) = k(\mathbf{x}, r) \cdot d(\mathbf{x}, r)\,. \tag{7}$$

Figure 10(a) shows a surface affected by bubbles. The bubble no. 1 has the biggest radius, while the bubble no. 2 is a little smaller. The output $k(\mathbf{x}, r)$ of the correlation filter configured with the radius of bubble no. 1 is depicted in Fig. 10(b). A 3D representation of this image is plotted in Fig. 11 together with the corresponding signals $d(\mathbf{x}, r)$ and $k'(\mathbf{x}, r)$. This example shows clearly that in $k'(\mathbf{x}, r)$ the false positives have strongly been attenuated with respect to the true ones, so that the fused signal $k'(\mathbf{x}, r)$ represents a more distinct and cleaner result that $k(\mathbf{x}, r)$.

D. Interpretation

A preprocessed image containing a defect at the position $\mathbf{x}_0$ can be described by the following model:

$$\begin{aligned} g(\mathbf{x}) &= c \cdot o(\mathbf{x} - \mathbf{x}_0) + n(\mathbf{x}) \\ &= o(\mathbf{x}) * * \, c \cdot \delta(\mathbf{x} - \mathbf{x}_0) + n(\mathbf{x})\,, \end{aligned} \tag{8}$$

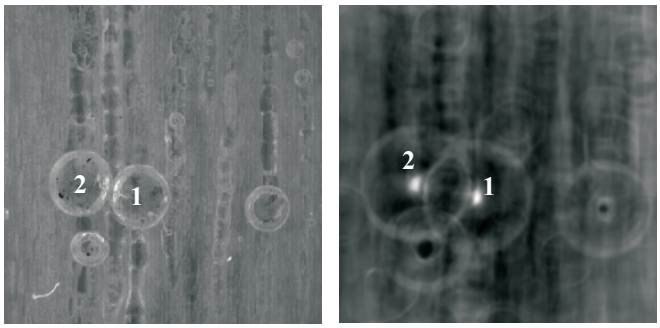

Fig. 10. (a) Varnished wood surface affected by bubbles (left). (b) Output of the correlation filter for r = 0.44 mm (right).

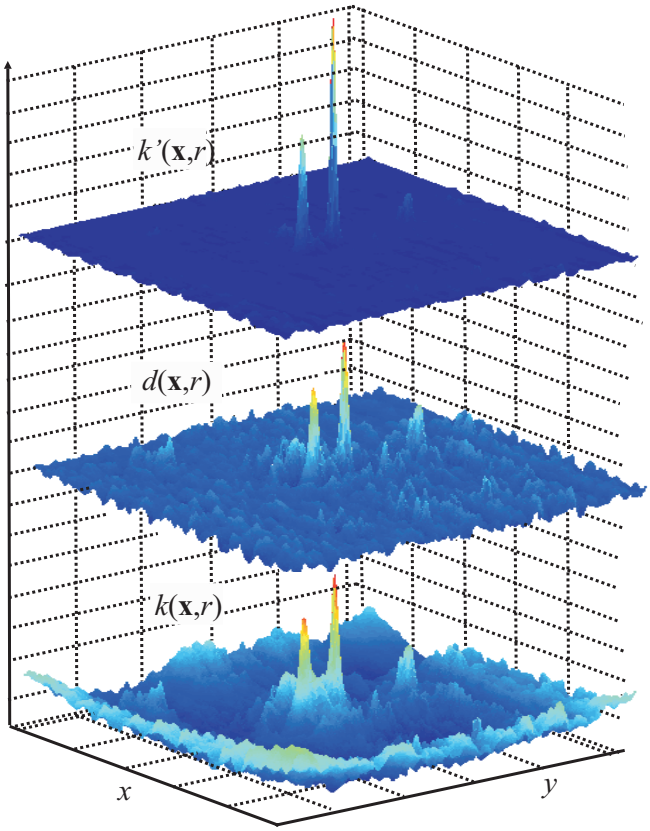

Fig. 11. Fusion of the detection filter outputs $k(\mathbf{x}, r)$ and $d(\mathbf{x}, r)$.

where $o(\mathbf{x})$ represents the defect, $\delta(\mathbf{x})$ the Dirac delta function, $n(\mathbf{x})$ a background noise, and $c > 0$ a constant. Thus, a filter yielding an impulse at the location $\mathbf{x}_0$ can be interpreted as an inverse filter $O^{-1}(\mathbf{f})$ to reconstruct the impulse function $\delta(\mathbf{x})$, where $O(\mathbf{f}) = \mathcal{F}\{o(\mathbf{x})\}$. Since $d(\mathbf{x}, r)$ features narrow impulses at the centres of the defects, the procedure used to compute this signal performs qualitatively an inverse filtering. Consequently, the proposed detection approach can be thought of as a fusion of the results of an inverse filter and a correlation filter.

E. Detection algorithm

To detect defects with different radii, the correlation filter is applied iteratively from the largest to the smallest radius;

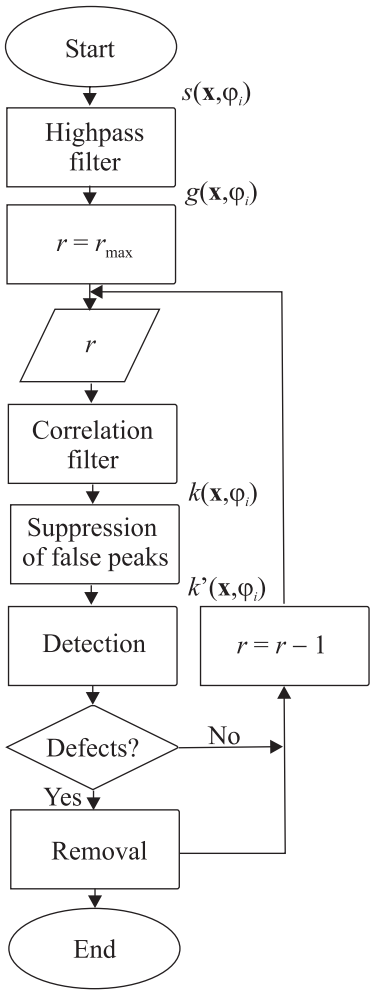

Fig. 12. Structure of the detection algorithm.

see Fig. 12. For each iteration, the template and the threshold must be reconfigured and the signal $d(\mathbf{x}, r)$ calculated.

If defects with a specific radius are detected, the corresponding areas are removed from the preprocessed image series $g(\mathbf{x}, \varphi_i)$ before the next iteration. The reason for this is that highlights near big defects can be interpreted as defects with smaller radii and may lead to false positives for smaller values of r. This is also the reason why the algorithm starts with the largest radius $r_{\max}$.

IV. Results

Several series of images of $B = 8$ pictures were taken with directional illumination from a flat elevation angle ($\Delta\varphi = 45°$, $\theta \approx 80°$). The tested surfaces are wood substrates from the furniture industry featuring a transparent varnish film.

The correlation results for different radii are shown in Fig. 13. The inspected surface shows two craters of different sizes. As depicted in Fig. 13, the small crater, which is hardly distinguishable from the background, could reliably be identified. In the right bottom picture, it is also evident that the big crater has been removed.

Figure 14(b) shows the output of the correlation filter for a radius of r = 0.12 mm for a wood surface affected by bubbles

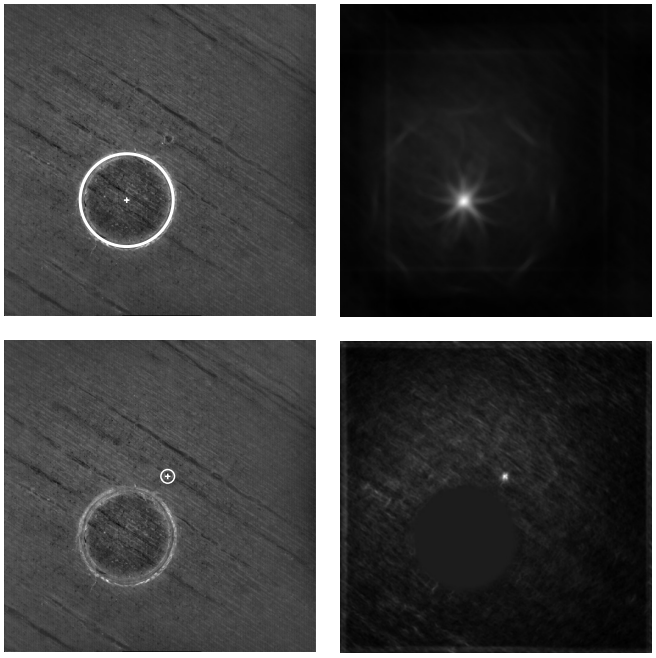

Fig. 13. (a) Varnished wood surface with craters (left). (b) Results of the correlation for two different radii (right).

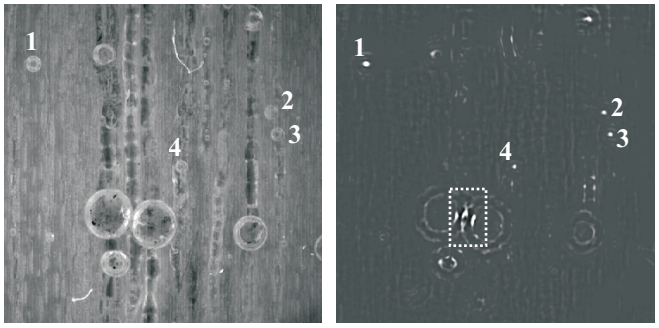

Fig. 14. (a) Varnished wood surface with bubbles (left). (b) Results of the correlation for r = 0.12 mm (right).

(a). The numeric references indicate the correspondence among the defects and the peaks in the correlation results. In this case the defects with radii greater than 0.12 mm were not removed after detection, and for this reason there are false positives on their borders (see the area inside the white rectangle). This example makes clear the necessity of removing the detected defects at the end of each iteration.

Figure 15 shows a surface with three detected craters and a 3D representation of the algorithm output for this test surface. This representation was obtained recording the normalized filter outputs $k(\mathbf{x}, r)$ for each iteration. The normalization of the filter outputs was accomplished by dividing them by a threshold which depends on r.

Three peaks exceed the normalized threshold (represented by the unitary cut plane), which means that there were three positive detections. The rest of the values, which correspond to intact varnish, significantly remains below the threshold. The surface under inspection shows the accurate

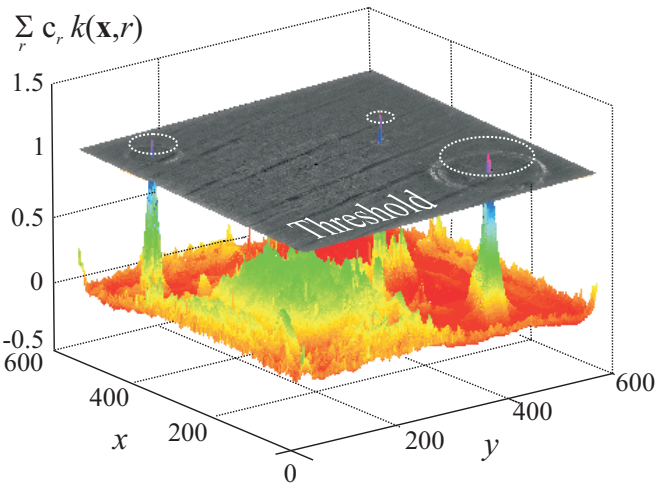

Fig. 15. Representation of the algorithm output.

correspondence between peak positions and defect centres.

V. Conclusion

A method to robustly detect circular defects on varnished or painted films has been presented. The partial visibility of these defects has been overcome by sampling the illumination space during the image acquisition. The result is an image series, along which the information of interest necessary for a reliable detection is distributed. Using knowledge on the morphology of the defects and the lighting direction, a correlation filter has been applied to the series of images. Thanks to a combination of this approach with an inverse filter, a significantly improved detection has been achieved.

To prove the robustness of our method, it has been tested on different wood substrates featuring a transparent varnish. This situation constitutes the most difficult case, not only due to the partly strong wood texture, but also because wood—as a natural material—has a high texture variability within and between species.

The results show the success of the method to detect circular defects of different sizes on arbitrary textures. Both the location and radius of the defects can be determined with an accuracy that is sufficient for all quality control needs.

References

[1] M. Scheithauer and H.J. Sirch, *Filmfehler an Holzlacken*, Institut für Holztechnologie Dresden, Vicentz-Verlag, 1996.

[2] R.M. Pérez Campos, V.P. Navarro Miquel, and F.J. Puchades, *Defects in coating furniture*, ISBN 84-922988-3-9, 1999.

[3] R.M. Pérez Campos and V.P. Navarro Miquel, *Stain of the wood: problems, solutions and process improvement*, ISBN 84-95077-00-0, 1999.

[4] F. Puente León, *Automatische Identifikation von Schußwaffen*, VDI-Verlag, Düsseldorf, 1999.

[5] C. Lindner and F. Puente León, "Segmentierung strukturierter Oberflächen mittels variabler Beleuchtung," *Technisches Messen*, vol. 73, no. 4, pp. 200–207, 2006.

[6] J. Beyerer and F. Puente León, "Suppression of inhomogeneities in images of textured surfaces," *Optical Engineering*, vol. 36, no. 1, pp. 85–93, 1997.

[7] K. R. Castleman, *Digital Image Processing*, Prentice-Hall, Englewood Cliffs, 1996.

[8] K. Kroschel, *Statistische Informationstechnik*, Springer, Berlin, 2004.